Fe(Se,Te) coated conductors deposited on simple RABiTS templates

G. Sylva[1,2], A. Augieri[3], A. Mancini[3], A. Vannozzi[3], G. Celentano[3], E. Bellingeri[1], C. Ferdeghini[1], M. Putti[1,2], V. Braccini[1,*]

[1] CNR-SPIN, C.so F. M. Perrone, 24, 16152 Genova, Italy

[2] Physics Department, University of Genova, via Dodecaneso 33, 16146 Genova, Italy

[3] ENEA Frascati Research Centre, Via E. Fermi 45, 00044 Frascati, Italy

* valeria.braccini@spin.cnr.it

Abstract

In this paper the feasibility of Fe(Se,Te) Coated Conductors (CC) on simple Rolling-Assisted Biaxilly Textured Substrate (RABiTS) template is studied. Starting from commercially available NiW5% tapes from Evico which have an out-of-plane orientation of about 6° and an in-plane orientation of 5.3°, a RABiTS template for Fe(Se,Te) coated conductors was realized depositing CeO_2 thin films on the metallic tape. The oxide buffer layers, deposited via Pulsed Laser Ablation, have an out-of-plane and an in-plane orientation suitable for Fe(Se,Te) deposition and act as a chemical barrier against Ni diffusion. The Fe(Se,Te) deposited on such a simple template show a superconducting transition T_c of 18 K, very high upper critical field values with a $\Delta T_{c,0}$ of only 3 K in 18 T and self-field transport isotropic critical current values of 10^5 A/cm^2 at 4.2 K, which is reduced of less than one order of magnitude up to 16 T.

1. Introduction

The Iron based superconductors (IBS) discovered ten years ago, which exhibit relatively high critical temperature T_c and huge upper critical field H_{c2}, have proved to have great potentiality for high field applications [1]. Among all the IBS families, the iron chalcogenides, also called the 11 ($FeSe_xTe_{1-x}$), are the simplest Iron Based Superconductors (IBS), and they are quite attractive because of their comparative ease of fabrication and the absence of toxic arsenic. 11 thin films have been successfully grown on single crystalline substrates [2,3] and on technical metallic templates made via IBAD [4] and on RABiTS [5] already available for the deposition of YBCO, showing values of critical current densities J_c as high as 10^5 A/cm^2 up to 30 T [5]. The route to the realization of long conductors is still long though. In IBS the exponential decay of J_c across misoriented grain boundaries seems to be less severe than for YBCO [6], the processing temperature is much lower than for YBCO and does not require oxygen: hence much simpler metallic substrates can be developed [7], reducing significantly the complexity and the manufacturing cost of IBS-CC, which may make them more attractive on the cost-performance basis.

We have studied the feasibility of producing 11 CCs by the deposition of thin films directly on a Ni/Fe alloy (namely, a biaxially oriented Invar 36 substrate) without any buffer layer but, despite the good orientation of the films, they did not show a superconducting transition due to a significant Ni diffusion from the substrate to the film [8,9].

In this work, we therefore tried the deposition of Fe(Se,Te) thin films on very simple RABiTS, i.e. NiW metallic tapes with a CeO_2 layer on top which can act also as a chemical barrier against Ni diffusion. In particular, we describe in this paper the deposition of CeO_2 buffer layer and Fe(Se,Te) thin films via PLD on NiW biaxially textured tapes. Moreover, a study of the texturing of both the buffer and the film and the characterization of the superconducting properties of the CC such as upper critical field and critical current up to 18 T was performed.

2. Experimental details

The commercially available cube textured Ni - 5% at.W (NiW) tapes from Evico were used as substrate for the development of Fe(Se,Te) (FST) CC [10]. The CeO_2 films, employed as a buffer layer, were deposited by pulsed laser deposition (PLD) technique using the 266 nm emission of a Nd:YAG solid state laser. Laser fluence was set at about 3 J/cm^2, and a repetition rate of 3 Hz was used. The target-to-substrate distance was fixed at 4.7 cm. Stoichiometric high density sintered target with purity of 99.99% was used as starting material. Prior to film deposition, NiW tape was annealed at 750 °C for 1 h in vacuum, i.e. in a background pressure lower of 1×10^{-6} mbar. CeO_2 layer was deposited at T_d = 600 °C in a two-step process [11] . In the first 10% of

the deposition time, the film was grown in vacuum. In the remaining deposition time, 10 mbar O_2 flowing atmosphere was introduced in the deposition chamber. The deposition time is fixed in order to obtain a 250 nm thick film. The sample is cooled down to room temperature in vacuum at a rate of 10 °C/min.

FST thin films about 150 nm thick were deposited on the metallic templates NiW / CeO_2 in an ultra-high vacuum PLD system equipped with a Nd:YAG laser at 1024 nm using a target with a nominal composition $FeSe_{0.5}Te_{0.5}$ prepared by direct synthesis with a two-step method [12]. The deposition was carried out at a residual gas pressure of 10^{-8} mbar while the template was kept at around 320 °C. The parameters of the laser used during the deposition are 3 Hz as laser repetition rate, 2 J/cm^2 as laser fluency (2 mm^2 spot size) and 5 cm as distance between target and sample [13]. The thickness of the films was controlled by the deposition time.

The structural characterization was performed by X-ray diffraction (XRD) using a Rigaku DMAX diffractometer for the buffer layers and a four-circle Siemens Kristalloflex 810 (Cu Kα radiation) and a PANanalytical Mod X'PERT PRO two-circle diffractometer for the thin films, in order to identify their purity, crystal structure and orientation, both in- and out-of-plane.

The temperature dependence of the electrical resistivity and the *I-V* curves have been acquired by the four probe method with a d.c. electrical probe mounted in a closed circuit He gas flow, cryo-free system provided with an 18 T superconducting magnet. In order to extract the critical current density (J_c) and the resistivity (ρ) values from the electrical transport measurements, a 1 mm wide and 3 mm long strip was obtained on the sample with standard U.V. photolithographic technique and wet etching in a dilute nitric acid solution in oxygen peroxide. A gold film, about 1 μm thick, was deposited on the electrical pads with the standard lift-off technique to reduce the contact resistance. The transport properties were characterized as a function of the temperature and applied magnetic field in two different configurations: magnetic field direction orthogonal and parallel to the tape surface, always keeping the maximum Lorentz force configuration (current orthogonal to the magnetic field). The critical current values were evaluated with the standard 1μV cm^{-1} criterion.

Surface analysis has been performed using a Park Systems XE-150 Atomic Force Microscope (AFM) operating in non-contact mode. Pre-mounted non-contact, high-resolution cantilever working at 309 MHz with nominal tip radius below 10 nm has been used. Images were flattened by subtracting a linear background for the fast scan direction and a quadratic background for the slow scan direction.

Microstructural investigations have been carried out by electron backscattering diffraction (EBSD) using an Oxford Nordlys Nano EBSD system installed on a Leo 1525 field-emission scanning electron microscope (SEM). Kikuchi patterns were acquired and indexed using Oxford AZtec software. For EBSD maps, the region of interest was sampled using a square grid with a pixel size of 25 μm^2. Tilt correction was applied. The microstructure of FST and CeO_2 films has been analyzed inside and outside the patterned strip used for transport measurement, respectively. EBSD misorientation maps and pole figures were generated using HKL Channel 5 software. Noise reduction been performed by extrapolating both zero solutions and wild spikes.

3. Results and discussion

3.1. CeO_2 buffer layer

In Figure 1, the XRD analysis for a CeO_2 buffer layer is reported. The intense (002) CeO_2 peak, the only reflection related to the film, indicates that the buffer layer develops a single orientation with the (001) direction perpendicular to the substrate. Even if a major part of the deposition process occurs in an oxygen atmosphere, peaks related to the substrate oxidation are not detectable. The ω-scans in the rolling direction through the (002) CeO_2 and (002) NiW peaks are reported in the insets. The value of FWHM of the CeO_2 films is of about 4°, a lower value with respect to the substrate, i.e. 6.6° confirming, as previously reported, that

CeO_2 films are prone to improve the out-of-plane substrate texture [14]. The CeO_2 film texture analyzed by pole figures in Figure 2 reveals the in-plane epitaxial relationship: [100] NiW// [110] CeO_2. The FWHM value of the φ-scan across the (111) CeO_2 poles is of about 5.2 - 7.4 °, a similar value is measured across the (111) NiW poles of the substrate as will be shown later. Figure 3 shows the SEM micrographs of a CeO_2/NiW buffer layer surface after the in-vacuum annealing process at a 600 °C for 5 minutes using a ramp rate of 60 °C/min. The annealing conditions have been selected in order to over simulate either the temperature or the ramp rate conditions used for the Fe (Se,Te) film. The CeO_2 film structural and morphological properties are unchanged after the annealing: in particular, the surface is uniform, smooth and dense. Above all, the CeO_2 film assures a good coverage of the grooves among the substrate grain boundaries of the substrate. This result shows that CeO_2 film on NiW is a robust template suitable for the FST film deposition.

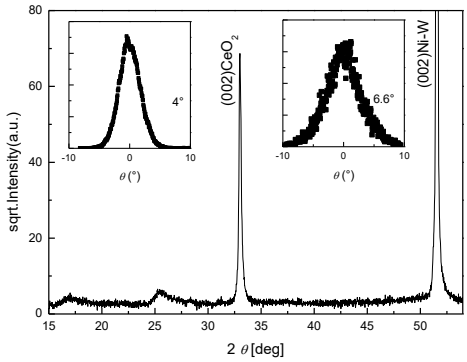

Figure 1: ϑ-2ϑ scan of CeO_2/NiW buffer layer structure. In the insets the (002) CeO_2 and (002) NiW rocking curves are reported

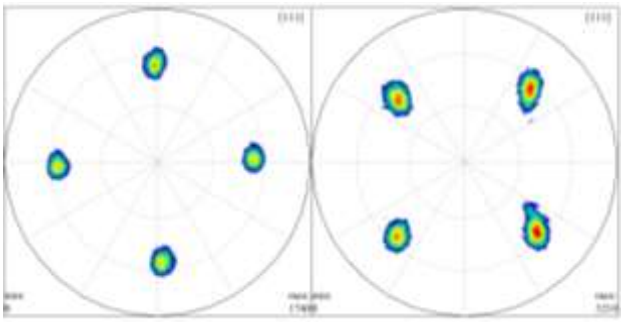

Figure 2: Pole figure along (111) direction of CeO_2 (left) and of NiW5% (right)

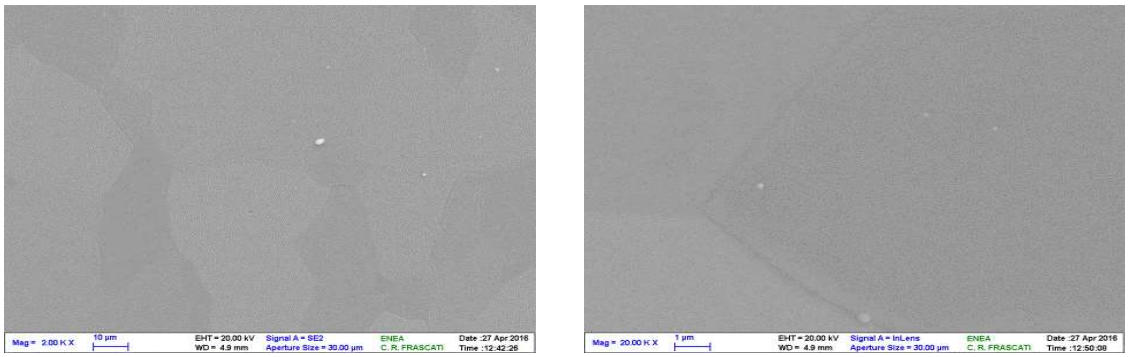

Figure 3: SEM images of the CeO_2 film grown on NiW after the annealing in vacuum condition at 600 °C for 5 minutes.

3.2. Fe(Se,Te) coated conductors

Figure (a) shows a θ-2θ scan of a FST thin film deposited onto the CeO_2/NiW template. Besides the (00l) peaks corresponding to the FST phase, the peaks coming from the template are clearly visible, but no other peaks are present relative to other orientations or phases, indicating an optimum *c*-axis alignment of the growth and a high purity of the phase. θ scan on the (001) peaks, reported in Figure (b), show FWHM values Δθ of about 3° in both the Rolling Direction (RD) and the Transverse Direction (TD), which are somehow lower than the values measured in the CeO_2 buffer layer and confirm a very good out-of-plane texture. In order to establish the in-plane epitaxy of the growth, φ scans of the (101) reflections of the FST films were performed. In Figure a the polar figures of FST along the (101) and the (111) direction are showed. While Figure b reports the φ scans of the (101) peak from the thin film are shown and compared with those of the (111) peak of the CeO_2 and the NiW substrate. The lattice of the FST thin film is aligned cube-on-cube with the NiW substrate and rotated by 45° in the *ab* plane compared that of the CeO_2 buffer layer, as it happens when FST thin films are grown on CaF_2 single crystals [15] and as it was already reported for the growth of FST thin films on RABiTS templates [5]. In fact, the diagonal of the lattice parameter of CeO_2 (and CaF_2) is about 3.82 Å (~ 5.41/√2), which matches exactly with the *a* lattice parameter of the FST. The average in-plane FWHM $\Delta\varphi_{FST}$ is about 4.9°, slightly higher than $\Delta\varphi_{CeO2}$ which is about 4.7°. Therefore, we can conclude that the FST thin films grown on CeO_2/NiW templates possess a good biaxial texturing determined by the texturing of the CeO_2 buffer layer.

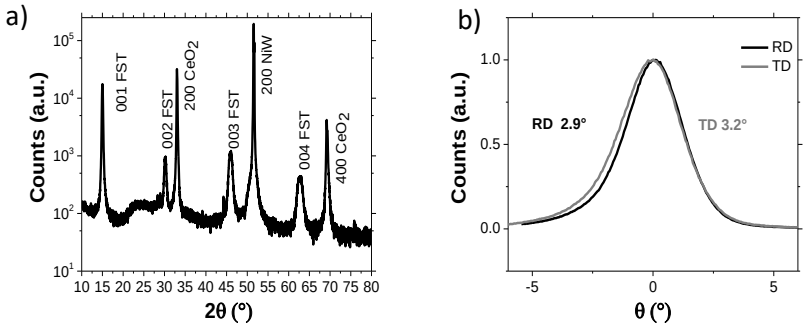

Figure 4: a) ϑ-2ϑ scan of the coated conductor with highlighted the (00l) peaks of template and FST film; **b)** rocking curve of the (001) peak of the FST thin film both in the Rolling and Transverse Direction with respect to the deformation; **c)** φ scans of the (111) peaks of CeO_2 and NiW and of the (101) peak of the FST thin film

Such results are consistent with the data reported in literature on IBAD templates[4][12] and RABiTS with CeO_2/YSZ/Y_2O_3 buffer layer [17].

Figure 4 shows the surface of a patterned FST film grown on CeO_2-buffered NiW substrate. The surface is uniform and shows an irregular hill-and-valley morphology. Average and rms roughness on 1 μm^2 area are 0.7 nm and 0.9 nm, respectively, slightly larger than values observed for CeO_2 film (0.4 and 0.5 nm, for average and rms roughness, respectively).

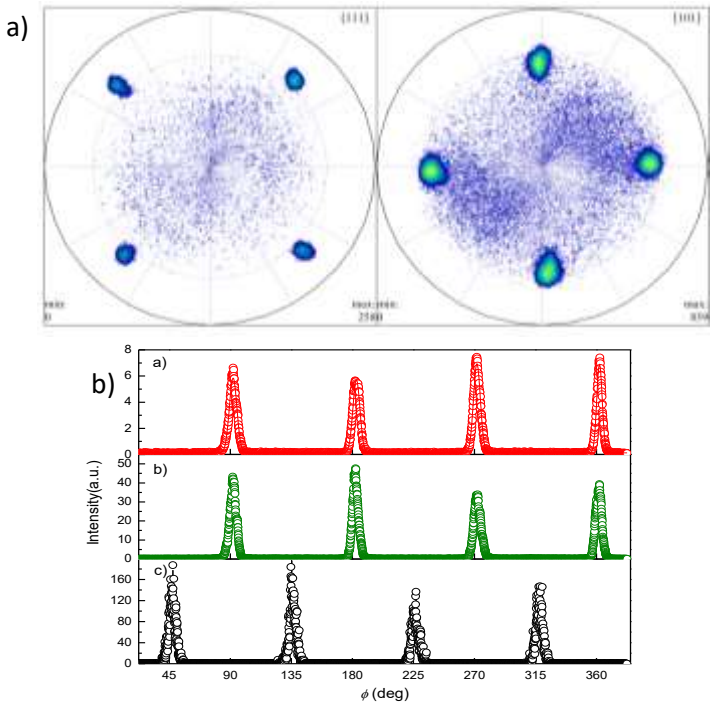

Figure 5: a) Polar figures of FST thin film made along (111) direction (left) and along (101) direction (right); **b)**φ scans of the(101) peak of the FST in red with FWHM=4.9°, of the (111) peaks of CeO_2 in green with FWHM= 4.7° and and of the (101) peak of NiW in black with FWHM= 5.3° .

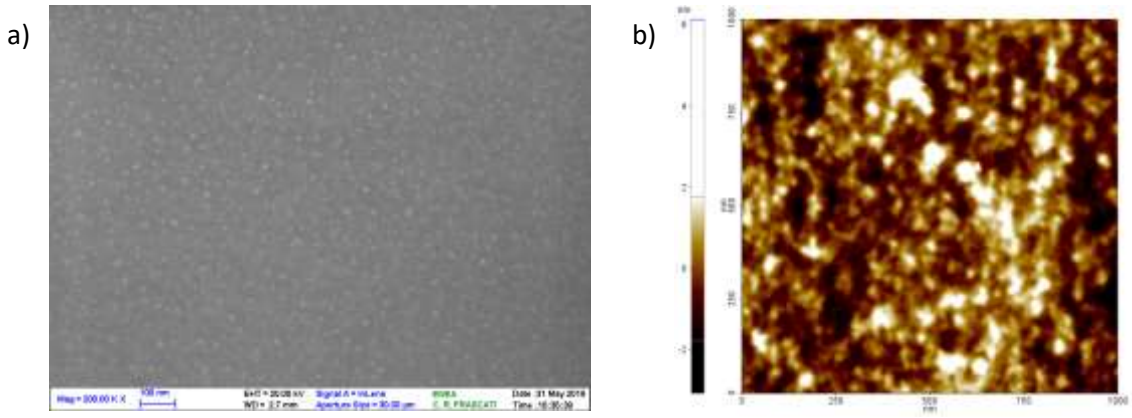

Figure 4: SEM (a) and AFM (b) images of patterned FST film grown on CeO_2-buffered Ni-W substrate.

The microstructure of the FST film was investigated by means of EBSD technique. Figure 5 shows the EBSD map (a) and the corresponding pole figures (b) of a FST film grown on CeO_2/Ni-W template. In both EBSD map and pole figures, points are displayed according to the local misorientation angle with respect to the ideal {001}<010> orientation, as shown in the legend of Figure 5c). In addition, gain boundaries above 2° and 10° (thin and thick lines, respectively) are shown.

Kikuchi patterns were well fitted using FeTe 4/mmm tetragonal phase. As can be seen, the FST film shows a sharp {001}<010> texture, with a fraction of oriented points of 98.9 % within 10 °. The FST film reproduces the microstructure of the underlying Ni-W substrate, as typically observed in RABiTS-based coated conductors [17]. In fact, the film shows a relative misorientation below 2° in regions of 35 ± 15 μm, which is the typical grain size of Ni-W RABiT substrate[11,18–20]. As can be seen, the vast majority of grain boundaries is below 10°. The microstructure is well-connected, with the presence of several low-angle grain boundary percolation

paths. The critical angle for the existence of a percolative path across the sampled area is 4.5°. This is in line with the value obtained in the case of YBCO film grown on a similar template [21].

The same microstructure was observed in the underlying CeO_2 buffer layer. Figure 6 shows the EBSD map (a) and the corresponding pole figures (b) of the CeO_2 film analyzed outside the patterned strip used for transport measurements. As can be seen, CeO_2 film shows a strong {001}<110> texture, with a fraction of oriented points of 99.2% within 10°.

From EBSD microstructural investigation, we can conclude that an epitaxial relationship (001)[010] FST // (001)[110] CeO2 // (001)[100] Ni-W has been obtained.

a)

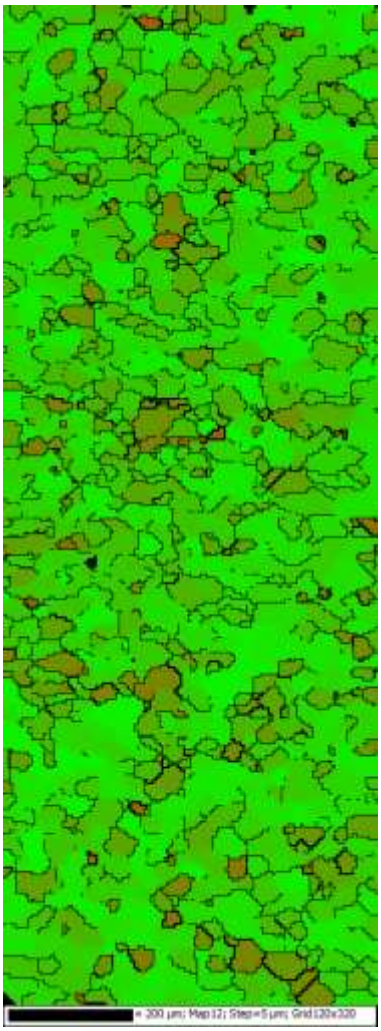

b)

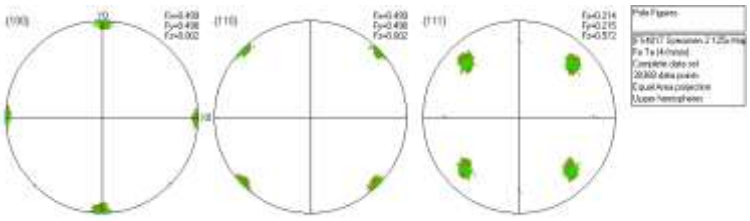

c)

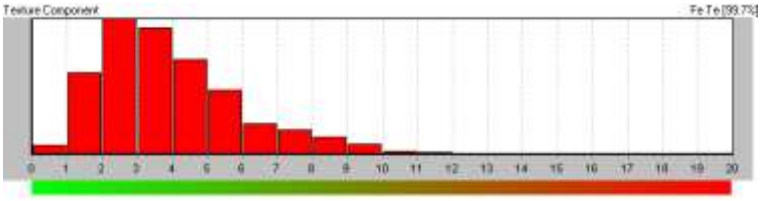

Figure 5: EBSD map (a) and pole figures (b) of FeSeTe film grown on CeO_2/Ni-W template. Kikuchi patterns have been indexed using FeTe 4/mmm tetragonal phase. The rolling direction is aligned horizontally. Points are displayed depending on their misorientation with respect to the ideal {001}<010> orientation, according to the legend (c). The legend shows the distribution of the acquired points with 1° class width as a function of the misorientation angle from 0° (green) to 20° (red). Points unindexed or above 20° are black. Grain boundaries above 2° (thin line) and 10° (thick line) are included in the map.

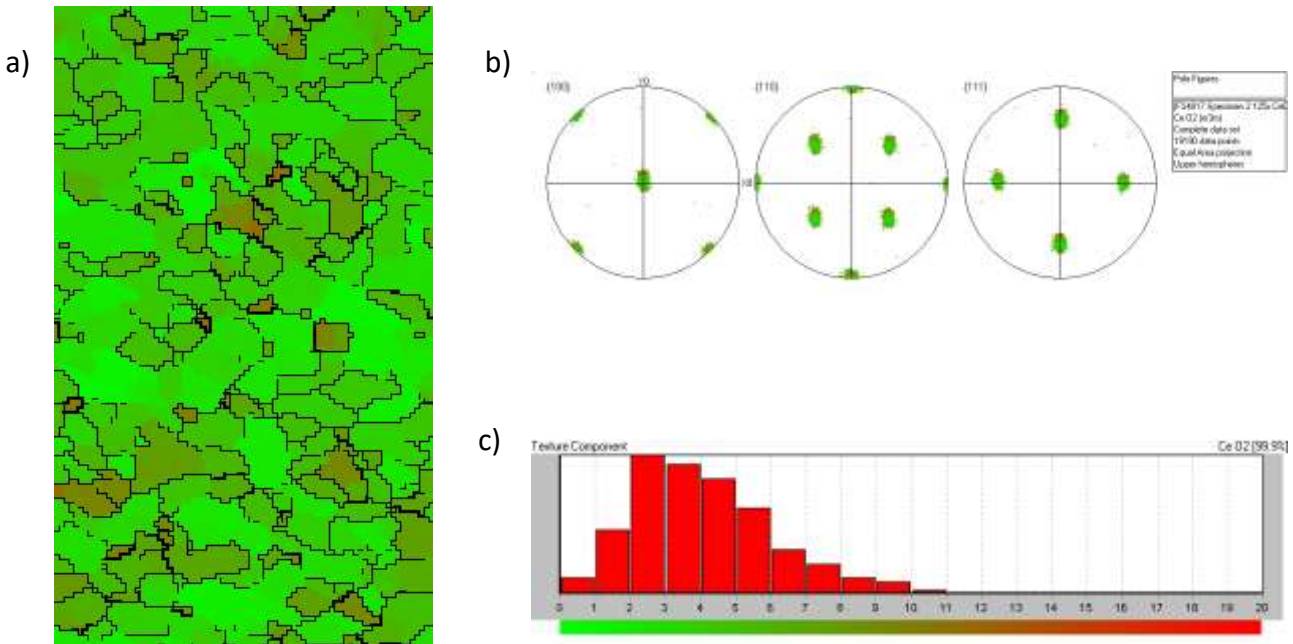

Figure 6: EBSD map (a) and pole figures (b) of CeO_2 film grown on Ni-W substrate, analyzed outside the patterned strip used for transport measurements. The rolling direction is aligned horizontally. Points are displayed depending on their misorientation with respect to the ideal {001}<110> orientation, according to the legend (c). The legend shows the distribution of the acquired points with 1° class width as a function of the misorientation angle from 0° (green) to 20° (red). Points unindexed or above 20° are black. Grain boundaries above 2° (thin line) and 10° (thick line) are included in the map.

In Figure 7 the temperature dependence of the normalized resistivity of the CC is shown up to 18 T in the two directions perpendicular and parallel to the magnetic field. $T_{c,0}$ is about 16 K with an onset above 18 K, comparable with thin films on single crystals or on technological templates[22].

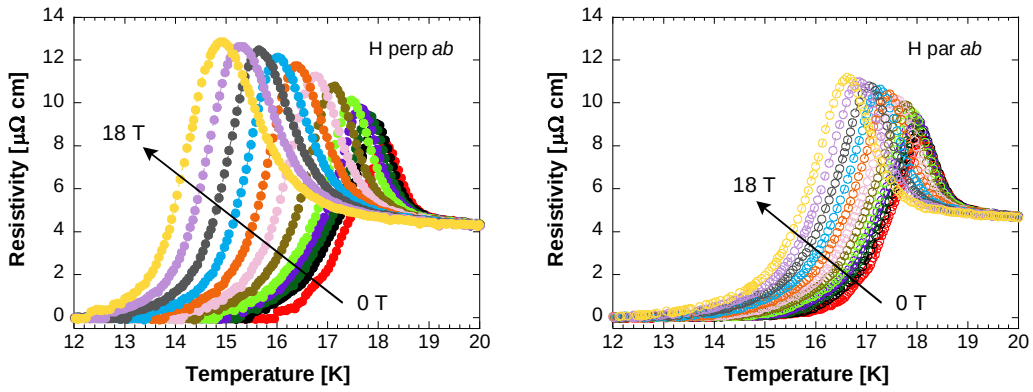

Figure 7: Resistivity as a function of the temperature for the FST film measured perpendicular and parallel to the magnetic field from 0 to 18 T (namely at 0, 1, 2, 3, 4, 6, 8, 10, 12, 14, 16, 18 T)

All the plotted $\rho(T)$ curves show low normal state resistivity values and an anomalous bump before the transition with a sharp increase in ρ followed by a steep reduction and then eventually reaching the zero resistance state. The maximum of the bump, T_m, shifts towards lower temperatures coherently with T_c as the applied magnetic field is increased.

The normal state temperature dependence of the resistivity exhibited by iron chalcogenides is, in general, not trivial. Semiconductor behaviour up to room temperature has been reported in both bulk and films, while a gradual crossover to metallic behaviour is usually observed for temperature approaching the superconducting transition [23–25]. These features give rise to highly non-linear $\rho(T)$ curves sometimes exhibiting local maxima. However, the presence of such a bump has never been reported in literature and was not observed in unpatterned films grown on the same template studied in the present work. On the other hand, similar behaviour of resistive transitions has been often reported for different superconducting films and has been ascribed to a phenomenon related to the current redistribution occurring in presence of film inhomogeneity (regions characterized by slightly different T_c and resistance value [26]. Therefore, this behavior is likely to be ascribed to a technological issue arisen during the film patterning process, coupled with some degree of film inhomogeneity. More detailed description of this behaviour through the use of an equivalent-circuit model is reported in Appendix 1.

The irreversibility field and the upper critical field values, H_{irr} and H_{c2}, are usually evaluated from the $R(T, H)$ curves using, respectively, the 10% and 90% of the superconductive transition criterion. This method cannot be applied to the measurements presented in this work since the reported anomalous behaviour, though accounted for by the presence of multiple path for the bias current, makes any evaluation of the normal state resistivity value quite speculative. The alternative criterion is thus adopted, associating $T_{c,0}(H)$ and $T_m(H)$ dependences to the H_{irr} and the H_{c2} curves, respectively. In the first case, the values will be close to those evaluated with the standard 10% criterion. In the upper critical field case, a qualitative picture of the $H_{c2}(T)$ dependence can be obtained, even though quantitatively underestimated (see Appendix1 for more details). .

In Figure 8 the H vs T diagram is reported, with the upper critical field H_{c2} and the irreversibility field H_{irr} calculated as reported above in both the field directions. H_{c2} vs T is very steep near T_c, with a downward curvature and slopes of about 63 T/K and 7 T/K in the parallel and perpendicular directions, respectively. Such values are quite high, even not as high as those observed in thin films deposited on single crystals which can reach up to 500 T/K and 30 T/K in the two directions [27]. The extremely high values reported on our strained film deposited on $LaAlO_3$ and CaF_2 were explained in terms of an extreme Pauli-limited $H_{c2}(T)$, indicative of the Fulde–Ferrell–Larkin–Ovchinnikov (FFLO) state [27]. The slopes near T_c are significantly higher than those reported on IBAD-LMO-buffered metal tapes [16]. Trying to estimate H_{c2} values at zero temperature, we applied the Werthamer-Helfand-Hohenberg relationship $H_{c2}(0) = -0.693 T_c (dH_{c2}/dT)_{|Tc}$ and obtained 790 T and 90 T for H // ab and H // c respectively. The anisotropy is not high: $H_{c2}^{//ab} / H_{c2}^{//c}$ is about 2.3 at 17 K while $H_{irr}^{//ab} / H_{irr}^{//c}$ is about 1.8 at 15 K, both higher though than the values reported in thin films grown on single crystals (where H_{c2} anisotropy can be as low as 1.2 [15]) and on IBAD-LMO-buffered metal tapes [16].

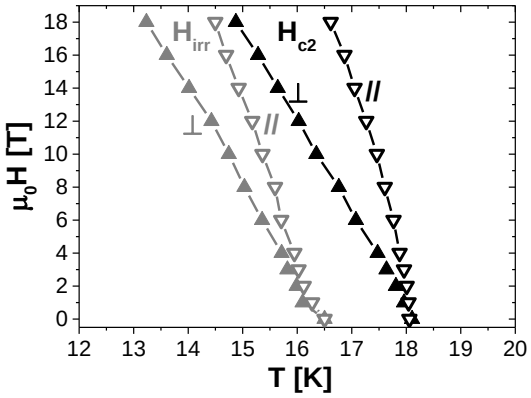

Figure 8: H-T diagram of the FST thin film. H_{c2} and H_{irr} are calculated from the $T_m(H)$ and $T_c(H)$ dependences, respectively

In **Errore. L'origine riferimento non è stata trovata.** a) we report the critical current density of the CC as a function of the magnetic field measured up to 18 T at 4.2 K and 9 K. Self-field J_c value at 4.2 K is above 1.0 10^5 A/cm^2 and above 2.0 10^4 A/cm^2 in fields up to 18 T, while the self-field J_c value at 9.0 K is above 5.0 10^4 A/cm^2. In **Errore. L'origine riferimento non è stata trovata.** b) the pinning force calculated from the J_c values are reported: at 4.2 K we are still far from its maximum at 18 T, while we observe a plateau starting from 14 T at 9 K.

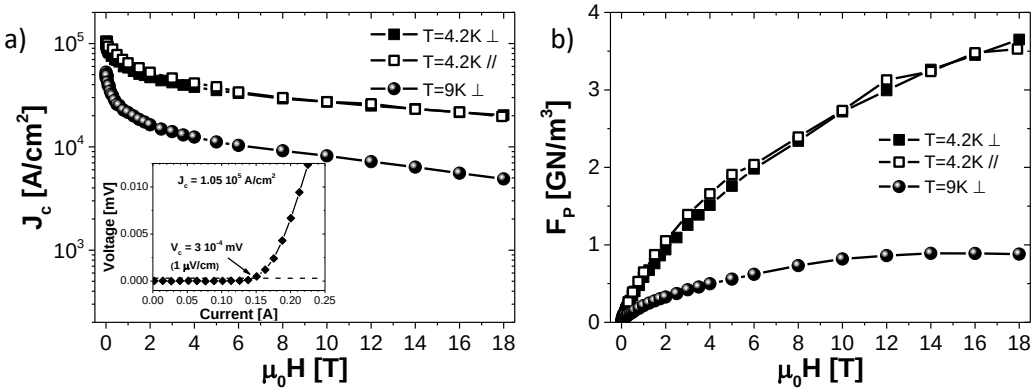

Figure 9: a) Transport J_c vs H at 4.2 K (both perpendicular and parallel to the magnetic field) and 9 K measured on the bridge. In the inset, the V-I curve at 0 T, 4.2 K with indication of the criterion for the J_c calcultation. **b)** Pinning force calculated from the critical current

Conclusions

The possibility to produce FST-CC on a simple RABiTS template made of NiW with a CeO_2 buffer layer, was presented in this paper. The NiW tape showed an in-plane and an out-of plane orientation suitable for FST thin film deposition, but the optimization of the texturing was obtained with the CeO_2 buffer layer which had a misorientation angle both in-plane and out-of-plane significantly lower than the critical angle above which the J_c in FST starts to decrease exponentially. The FST thin film was deposited through PLD on this simple RABiTS template and showed not only a texturing comparable to the substrates but also superconducting properties comparable to other CC realized with complex template. The superconducting transitions occurs at about 18 K, and the J_c at 4.2 K is above 1.0 10^5 A/cm^2 in self-field and above 2.0 10^4 A/cm^2 in fields up to 18 T. These results strengthen the possibility to produce simpler and cost-effective FST-CC, which can be appealing for large scale applications.

Appendix 1

Low normal state resistance values, in fact, can be predicted by assuming a multiple path for the bias current: one metallic path, characterized by electrical resistance R_m, in parallel with a superconducting path comprised of one or more phases, characterized by R_{sc}. The anomalous bump can be reproduced by assuming the superconducting path with two distinct regions connected in series: one characterized by R_{sc1}, and the other by $R_{sc2}>R_{sc1}$ [26]. This condition could have been caused during the not yet optimized patterning process: the Au film deposited on the current pads partially lie on the metallic substrate providing the alternative metallic path (R_m), while the pre-sputtering stage operated on the contact pads before the Au deposition could have created FeSeTe regions with resistance values (R_{sc2}) increased with respect to the strip (R_{sc1}).

It is easy to recognize that in this case, the measured resistance value, R_{exp}, obtained as V_{exp}/I_0 with I_0 as the bias current and V_{exp} as the voltage recorded across the superconducting strip, can be evaluated as [26]:

$$R_{exp} = (R_m R_{sc1})/(R_m+R_{sc1}+R_{sc2})$$

and does not correspond to the actual FeSeTe strip resistance, unless $R_{sc} = R_{sc1} + R_{sc2} << R_m$. Taking into account the typical resistivity values reported for NiW and FeSeTe materials [28,29], this condition will hold only close to the film transition temperature, $T \approx T_c$. On approaching the superconductive transition, the current flowing in the superconductive path increases before the complete transition to zero resistance takes place, determining the bump in the $\rho(T)$ curve.

In Figure A1, the measured zero-field $R(T)$ curve is plotted together with the R_{sc1} curve calculated as:

$$R_{sc1} = R_{exp} \times (R_m + R_{sc2})/(R_m - R_{exp}) \qquad \text{(A1)},$$

As can be seen, with a proper definition of R_{sc2} (dashed line), a monotonously decreasing resistive transition for R_{sc1} is recovered (continuous line). It has to be noticed that the upturn of the $R(T)$ curve at about 19 K corresponds to the onset of the R_{sc} transition and that the peak corresponds to the mid transition point. Finally, for temperatures close to T_c, $R_{sc} \approx R_{exp}$ (= $R(T)$) holds.

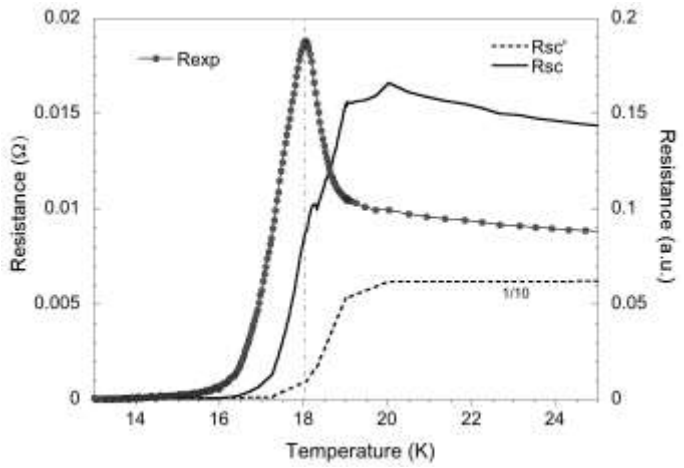

Figure A1. Experimental R(T) curve measured on patterned FeSeTe strip (dotted curve) and the actual strip resistance, R_{sc1}, calculated with eq. (A1) (continuous curve). The vertical dash-dotted line at T_m temperature corresponding to the R(T) bump maximum, is also drawn. See text for more details.

References

[1] Pallecchi I, Eisterer M, Malagoli A and Putti M 2015 Application potential of Fe-based superconductors *Superconductor Science and Technology* **28** 114005

[2] Braccini V, Kawale S, Reich E, Bellingeri E, Pellegrino L, Sala A, Putti M, Higashikawa K, Kiss T, Holzapfel B and Ferdeghini C 2013 Highly effective and isotropic pinning in epitaxial Fe(Se,Te) thin films grown on CaF_2 substrates *Applied Physics Letters* **103** 172601

[3] Bellingeri E, Pallecchi I, Buzio R, Gerbi A, Marrè D, Cimberle M R, Tropeano M, Putti M, Palenzona A and Ferdeghini C 2010 Tc=21 K in epitaxial FeSe0.5Te0.5 thin films with biaxial compressive strain *Applied Physics Letters* **96** 102512

[4] Si W, Zhou J, Jie Q, Dimitrov I, Solovyov V, Johnson P D, Jaroszynski J, Matias V, Sheehan C and Li Q 2011 Iron-chalcogenide $FeSe_{0.5}Te_{0.5}$ coated superconducting tapes for high field applications *Applied Physics Letters* **98** 262509

[5] Si W, Han S J, Shi X, Ehrlich S N, Jaroszynski J, Goyal A and Li Q 2013 High current superconductivity in FeSe0.5Te0.5-coated conductors at 30 tesla *Nature Communications* **4**

[6] Katase T, Ishimaru Y, Tsukamoto A, Hiramatsu H, Kamiya T, Tanabe K and Hosono H 2011 Advantageous grain boundaries in iron pnictide superconductors *Nature Communications* **2**

[7] Huang J, Chen L, Jian J, Khatkhatay F, Jacob C and Wang H 2015 A simplified superconducting coated conductor design with Fe-based superconductors on glass and flexible metallic substrates *Journal of Alloys and Compounds* **647** 380–5

[8] Palombo M, Malagoli A, Pani M, Bernini C, Manfrinetti P, Palenzona A and Putti M 2015 Exploring the feasibility of Fe(Se,Te) conductors by *ex-situ* powder-in-tube method *Journal of Applied Physics* **117** 213903

[9] Sylva G, Malagoli A, Bellingeri E, Putti M, Ferdeghini C, Vannozzi A, Celentano G, Hopkins S.C, Lunt A.J.G, Ballarino A, and Braccini V Analysis of Fe(Se,Te) Films Deposited on Unbuffered Invar 36

[10] http://www.evico.de/

[11] Varesi E, Celentano G, Petrisor T, Boffa V, Ciontea L, Galluzzi V, Gambardella U, Mancini A, Rufoloni A and Vannozzi A 2003 Pulsed laser deposition of high critical current density $YBa_2Cu_3O_{7-x}$/CeO_2/Ni W architecture for coated conductors applications *Superconductor Science and Technology* **16** 498–505

[12] Palenzona A, Sala A, Bernini C, Braccini V, Cimberle M R, Ferdeghini C, Lamura G, Martinelli A, Pallecchi I, Romano G, Tropeano M, Fittipaldi R, Vecchione A, Polyanskii A, Kametani F and Putti M 2012 A new approach for improving global critical current density in $Fe(Se_{0.5}Te_{0.5})$ polycrystalline materials *Superconductor Science and Technology* **25** 115018

[13] Bellingeri E, Kawale S, Caglieris F, Braccini V, Lamura G, Pellegrino L, Sala A, Putti M, Ferdeghini C, Jost A, Zeitler U, Tarantini C and Jaroszynski J 2014 High field vortex phase diagram of Fe(Se, Te) thin films *Superconductor Science and Technology* **27** 044007

[14] Budai J D, Yang W, Tamura N, Chung J-S, Tischler J Z, Larson B C, Ice G E, Park C and Norton D P 2003 X-ray microdiffraction study of growth modes and crystallographic tilts in oxide films on metal substrates *Nature Materials* **2** 487–92

[15] Bellingeri E, Kawale S, Braccini V, Buzio R, Gerbi A, Martinelli A, Putti M, Pallecchi I, Balestrino G, Tebano A and Ferdeghini C 2012 Tuning of the superconducting properties of $FeSe_{0.5}Te_{0.5}$ thin films through the substrate effect *Superconductor Science and Technology* **25** 084022

[16] Xu Z, Yuan P, Ma Y and Cai C 2017 High-performance $FeSe_{0.5}Te_{0.5}$ thin films fabricated on less-well-textured flexible coated conductor templates *Superconductor Science and Technology* **30** 035003

[17] Feldmann D M, Holesinger T G, Cantoni C, Feenstra R, Nelson N A, Larbalestier D C, Verebelyi D T, Li X and Rupich M 2006 Grain orientations and grain boundary networks of $YBa_2Cu_3O_{7-\delta}$ films deposited by metalorganic and pulsed laser deposition on biaxially textured Ni–W substrates *Journal of Materials Research* **21** 923–34

[18] Eickemeyer J, Selbmann D, Opitz R, Wendrock H, Maher E, Miller U and Prusseit W 2002 Highly cube textured Ni–W-RABiTS tapes for YBCO coated conductors *Physica C: Superconductivity* **372**–**376** 814–7

[19] Kim K T, Lim J H, Kim J H, Jang S H, Joo J, Kim C-J, Song K J and Shin H S 2005 Effect of W Addition on the Microstructure and Properties of Ni-W Substrates for Coated Conductors *IEEE Transactions on Appiled Superconductivity* **15** 2683–6

[20] Vannozzi A, Rufoloni A, Celentano G, Augieri A, Ciontea L, Fabbri F, Galluzzi V, Gambardella U, Mancini A and Petrisor T 2006 Cube-textured substrates for YBCO-coated conductors: microstructure evolution and stability *Superconductor Science and Technology* **19** 1240–5

[21] Celentano G, Galluzzi V, Mancini A, Rufoloni A, Vannozzi A, Augieri A, Petrisor T, Ciontea L, Tuissi A, Villa E and Gambardella U 2005 YBCO films and CeO/sub 2//YSZ/CeO/sub 2/ buffer layers grown on Ni-Cr-W RABiTS with a Pd seed layer *IEEE Transactions on Appiled Superconductivity* **15** 2691–4

[22] Sakoda M, Iida K and Naito M 2018 Recent progress in thin-film growth of Fe-based superconductors: superior superconductivity achieved by thin films *Superconductor Science and Technology* **31** 093001

[23] Li Q, Si W and Dimitrov I K 2011 Films of iron chalcogenide superconductors *Reports on Progress in Physics* **74** 124510

[24] Si W, Jie Q, Wu L, Zhou J, Gu G, Johnson P D and Li Q 2010 Superconductivity in epitaxial thin films of Fe 1.08 Te : O x *Physical Review B* **81**

[25] Mele P 2012 Superconducting properties of iron chalcogenide thin films *Science and Technology of Advanced Materials* **13** 054301

[26] Vaglio R, Attanasio C, Maritato L and Ruosi A 1993 Explanation of the resistance-peak anomaly in nonhomogeneous superconductors *Physical Review B* **47** 15302–3

[27] Tarantini C, Gurevich A, Jaroszynski J, Balakirev F, Bellingeri E, Pallecchi I, Ferdeghini C, Shen B, Wen H H and Larbalestier D C 2011 Significant enhancement of upper critical fields by doping and strain in iron-based superconductors *Physical Review B* **84**

[28] Si W, Lin Z-W, Jie Q, Yin W-G, Zhou J, Gu G, Johnson P D and Li Q 2009 Enhanced superconducting transition temperature in FeSe0.5Te0.5 thin films *Applied Physics Letters* **95** 052504

[29] Vannozzi A, Thalmaier G, Armenio A A, Augieri A, Galluzzi V, Mancini A, Rufoloni A, Petrisor T and Celentano G 2010 Development and characterization of cube-textured Ni–Cu–Co substrates for YBCO-coated conductors *Acta Materialia* **58** 910–8